



Vertical Projectile Launcher for Study of Rapid Penetration into Soil Targets

L. Giacomo¹ · D. Grace¹ · M. Omidvar¹ · S. Bless¹ · M. Iskander¹

Received: 1 December 2023 / Accepted: 16 June 2024
© The Society for Experimental Mechanics, Inc 2024

Abstract

The majority of ballistic experiments in granular media in the literature involve horizontally launching projectiles. Notwithstanding the significant scientific findings resulting from these studies, the depth-dependence of geostatic stresses is not captured in a horizontal configuration. The design and performance of a vertical ballistic range is described herein. The range is capable of launching projectiles at impact speeds of up to 900 m/s into soil targets. A pluviator is employed to prepare sand targets with precise and highly repeatable bulk densities. Use of a photon Doppler velocimeter (PDV) and other instrumentation to track projectile velocity both in-flight and during penetration into the soil target are elucidated. A relationship is found between the muzzle velocity and chamber pressure. Launcher performance is quantified by comparing measured muzzle velocities with theoretical velocities calculated from isentropic expansion of gas behind the projectile in the launcher barrel. It is found that the launcher efficiency is in the range of 70 to 90%, with efficiency increasing for heavier projectiles. The PDV instrumentation developed for the range successfully resolves projectile velocities in flight and during penetration into the soil target.

Keywords Launcher · Compressed gas gun · Sand penetration · Photon Doppler velocimetry

Introduction and Background

Projectile penetration testing in granular materials has been extensively studied in the past [1–3]. A wide range of military and civilian applications benefit from study of the topic, including design of earth penetrating projectiles, cleanup of military ranges from unexploded ordnance (UxO), planetary impact, and design of foundations of offshore oil platforms, among others. Subscale laboratory experiments are often carried out to study soil response to projectile penetration in lieu of costly full-scale field experiments. Projectiles are launched into soil targets at impact velocities ranging from tens of meters per second to supersonic and hypersonic velocities, depending on the application. The design of the launcher depends on the desired impact velocities and test conditions.

Several launcher designs have been explored and documented in the literature [4]. These encompass spring and piston mechanisms, single and double-stage gas guns, and explosive acceleration techniques, each tailored to distinct objectives. Common among these designs is that they typically launch projectiles horizontally into targets [5–8]. However, in-situ stress fields within granular materials exhibit depth-dependence. Capturing this depth-dependent behavior is paramount when developing predictive models from subscale experiments, particularly those intended for engineering applications. Launching projectiles vertically into soil targets poses a unique set of challenges. A limited number of vertical designs have been reported in the literature. The NASA Ames Vertical Gun Range (AVGR) has been widely used for study of planetary impact physics for several decades [9]. The NASA Johnson Space Center Experimental Impact Laboratory also operates a vertical gun capable of launching projectiles for hypervelocity impact studies [10]. The Institute of Space and Astronautical Science at the Japan Aerospace Exploration Agency (JAXA) operates a two-stage vertical gas gun for space and planetary impact studies [11]. Price et al. [12] presented a unique vertical launcher, which featured a right angle-shaped design, and operated in

✉ M. Omidvar
omidvar@manhattan.edu

¹ Civil and Environmental Engineering Department,
Manhattan College, Riverdale, NY, USA

single-stage or two-stage modes to achieve impact velocity ranges of 0.3–2 km/s. Zhong et al. [13] used a single-stage gas gun to investigate vertical impact on carbonate sand targets at approximately 170 m/s. McDonnell (2006) described a launcher design which accommodated impact at all angles ranging from vertical and horizontal. In the present study, the design and construction of a dedicated vertical ballistic range is described for launching projectiles into a range of cohesionless and cohesive soil targets.

The impetus for the present work stems from the need for remediating unexploded ordnance (UxO) contamination in areas such as Formerly used Defense Sites (FUDS) and military ranges marked for transition to civilian use. The issue of buried UxO, a legacy of munitions development at military sites as well as their wartime deployment, presents a substantial global challenge. In the United States alone over 1,800 FUDS necessitating investigation and cleanup were identified as of a 2019 report to the US Congress [14, 15].

The design and performance of a laboratory projectile launcher capable of propelling small-diameter projectiles with speeds of up to 900 m/s into soil targets in a controlled and repeatable manner is documented in this paper. Details of the launcher design are presented, along with a thorough quantification of its efficiency and performance. Predictive equations for quantification of launcher efficiency are presented for design of similar launchers. The relatively simple design of the launcher combined with its high efficiency makes it a versatile tool for laboratory ballistic testing for a variety of scientific and engineering applications. It is shown that the projectile penetration tests carried out on sand targets using the launcher exhibit a high degree of repeatability. In the next sections, details of the launcher are presented, including its design, vertical mounting, methods to measure muzzle velocity, performance using projectiles ranging in mass from 16.4 g to 96.5 g, and corresponding efficiency calculations.

Design of Ballistic Launcher

The launcher was used to vertically propel projectiles into sandy targets prepared at precise densities. Although horizontal ballistic penetration tests in soil have resulted in significant findings, data produced from such experiments do not capture the vertical depth-dependence of soil behavior. Frictional granular materials exhibit a depth-dependence in shear strength. This behavior is further complicated by natural variations in stratigraphy resulting from sedimentation in natural soil deposits. Incorporation of the depth-dependence of soil response into investigation of rapid penetration in such materials is important in modeling and predicting the response and depth of burial (DoB). A vertical launcher was therefore designed for such purposes, as described in the following sections.

Launcher Components

Projectile launchers for laboratory testing can be divided into two broad categories [16]. These include spring-piston and reservoir launchers. The spring-piston launcher fires a projectile by using a mechanical spring and piston mechanism to compress gas directly behind the projectile, thereby providing the energy needed for launch. The reservoir launcher, which was the pressure supply mechanism selected in this study, relies on pressurized gas stored in a reservoir chamber. The reservoir-type launcher was selected due to its capability to vary the chamber pressure, allowing for an uncomplicated user control over the impact velocity. The launcher used to propel projectiles into soil targets was a custom-made single-stage high performance gas gun (Sydor Technologies). It was a horizontal-firing launcher custom-fitted for vertical mounting.

The launcher consisted of a number of interconnected components including the main gas chamber with an integrated shuttle valve, a breech where the projectile could be loaded, a barrel to accelerate the projectile, an electric trigger to activate a fast-acting electro-pneumatic solenoid valve, and a support structure, among others [17]. A schematic representation of the launcher system is shown in Fig. 1, along with close-up views of the main components.

Gas Chamber The main chamber of the launcher could be pressurized with air, helium, or nitrogen gas. In this study, ultra-high purity (UHP) helium was used because of its high sound speed and general availability. The reservoir consisted of a 147 cc steel chamber (Fig. 1c) with an integrated shuttle valve at its base. The pressure supplied to the reservoir was regulated using a fine-tuned regulator (Hale-Hamilton Valves LTD., GHP15 MK2) (Fig. 1a). Pressure gauges were mounted to the air and UHP helium reservoirs, both sides of the UHP helium supply regulator, and the launcher chamber, to monitor gas pressures in the system. A ball valve (HYDAC International, DN13 KHBSM-G1/2 PN500) was used to control gas flow into the launcher pressure reservoir and adjust pressures as needed. The ball valve was equipped with two limit switches (Telemecanique – XCXL) that served as a safety interlock system (Fig. 1b). The limit switches were equipped with two rollers that moved in and out of notches in the ball valve. The launcher could be triggered only when the ball valve was in the closed position.

Shuttle Valve The main feature of the launcher was a free-floating shuttle valve used within the reservoir. This design allowed for abrupt release of pressurized helium gas from the reservoir into the barrel. This sudden release of gas was critical for achieving high muzzle velocities. The operating mechanism of the shuttle valve is schematically

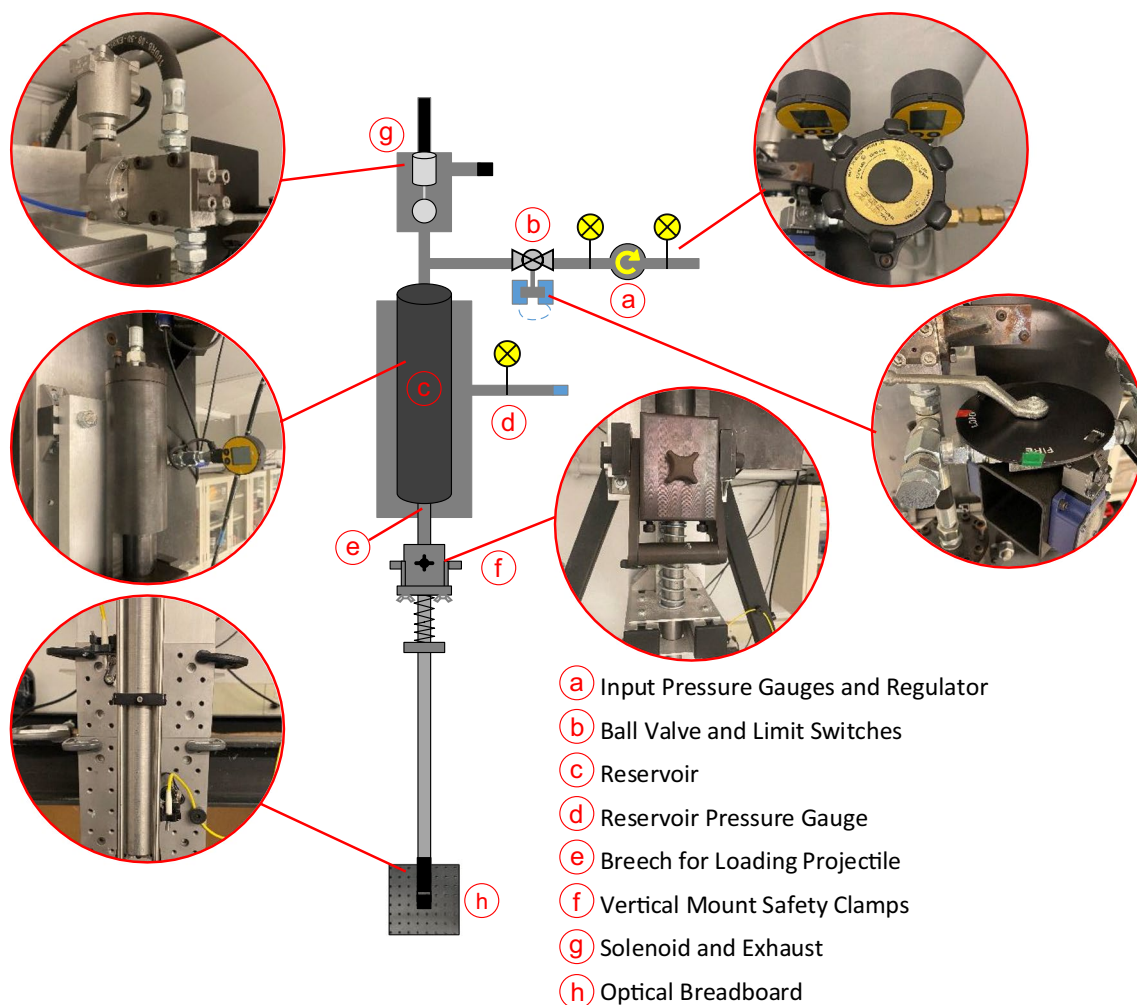


Fig. 1 Schematic drawing of the launcher components

demonstrated in Fig. 2. Initially, when the reservoir is depressurized, the shuttle valve rests freely along the inner guide tube. When pressure is introduced into the reservoir from the back end leading to the ball valve, the shuttle valve is pushed up against the front end of the cylinder, leading to the launcher breech. A minimum reservoir pressure of approximately 25 bar is required to seal the shuttle valve. Lower reservoir pressures can be used, but large leakage of gas from the shuttle valve results in low efficiency at these velocities. When the launcher firing mechanism is triggered, the solenoid valve leading to the back end of the reservoir is opened for a very short duration. This causes a sudden release of some gas from the reservoir and a drop in the reservoir pressure, thereby releasing the shuttle valve from its tight seal over the front of the reservoir. Consequently, the pressurized gas in the reservoir abruptly releases into the barrel through the breech. As noted above, the shuttle valve allowed for small leaks into the breech, which were not sufficient to propel the projectile. For example, pressure

drops of 1.25 bar/minute and 5.25 bar/minute were observed at reservoir pressures of 50 bar and 150 bar, respectively.

Breech A custom-made loading breech (Fig. 1e) with safety clamps was used to load projectiles into the barrel. A two-step clamp setup, comprising a barrel clamp and a safety clamp, shown in Fig. 1f, was used to lock the barrel in place. Two methods could be used for holding projectiles within the breech prior to launch (Fig. 3). A recess in the breech could be used to load projectiles using O-rings. Alternatively, it was found that 2-mm wide double-sided tape mounted on the outside of the projectile along its back rim provided sufficient support to hold the projectile in the breech prior to launch. The tape sheared off from the projectile, and remained within the breech upon launching the projectile. This ensured that the photon Doppler velocimeter (PDV) laser light path employed to track the motion of the projectile was not obstructed during experiments. The double-sided tape method was favored for these reasons.

Fig. 2 Schematic illustration of the stages of shuttle valve operating mechanism: (a) depressurized rest position; (b) pressurized reservoir prior to launch; (c) depressurized reservoir following solenoid trigger

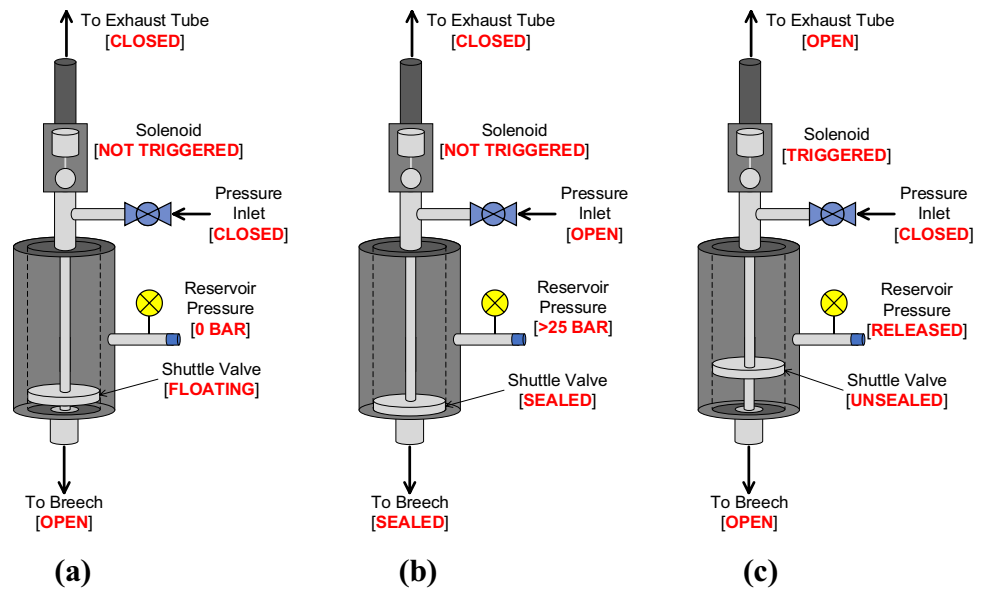
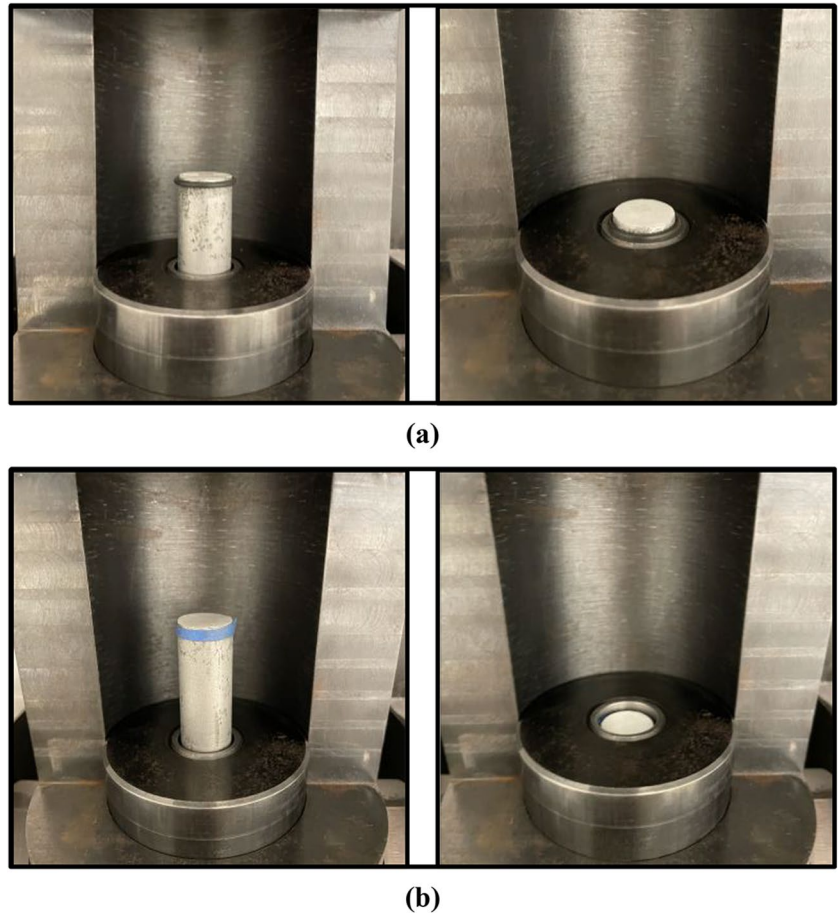


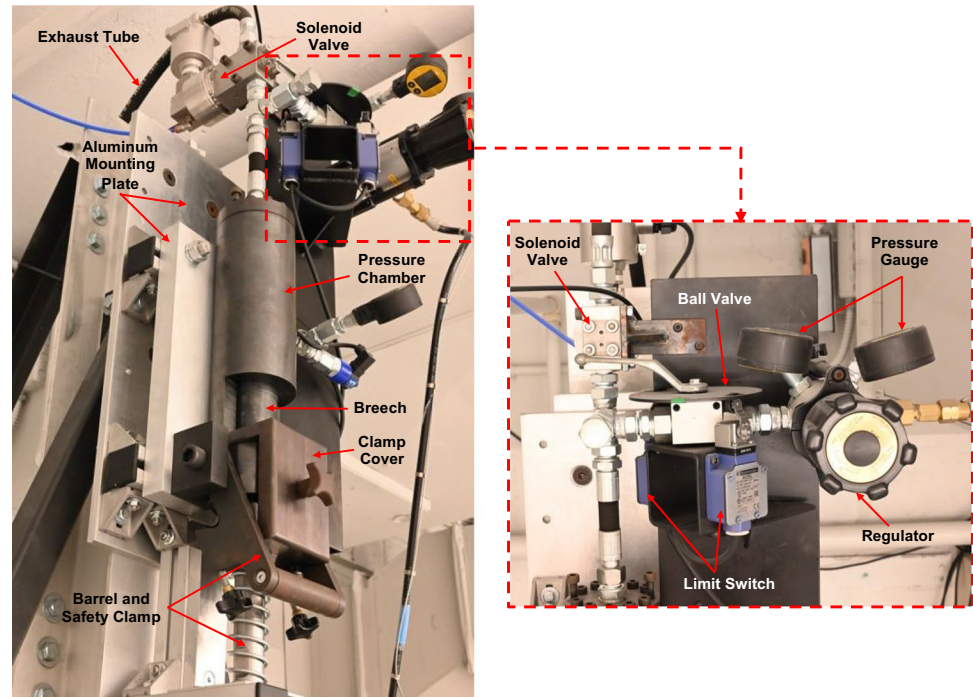
Fig. 3 Projectile loading mechanisms tested in this study. (a) O-ring; (b) Double-sided tape



Launcher Barrel The launcher barrel was 1.22 m long with a 14.40 mm inner diameter. The barrel threaded into a breech which facilitated loading of the projectile. A spring was added to the outside of the barrel below the breech to allow for

vertically loading projectiles into the breech (Fig. 4). Rod-cylindrical projectiles were used in this study. The inner bore of the barrel was smooth and was precision-machined to a diameter of 14.40 mm. Smaller diameter projectiles or non-cylindrical

Fig. 4 Components of the gas launcher



projectiles can be fired using a sabot and a sabot catcher. Flat-ended and conical nose projectiles having a diameter of 14.30 mm and a length-to-diameter ratio of 5.33 were used.

Trigger and Other Support Components The launcher was triggered electrically by a fast-acting electro-pneumatic solenoid (Bifold, FP03P). Dry compressed air was supplied to the solenoid at a regulated operating pressure of 8 bar. The launcher was custom-fitted with components to accommodate vertical mounting, such as a mounting plate, support base frame, barrel spring, and associated hardware. In addition, a support base frame was incorporated into the launcher to maintain the barrel in its vertical position, and to accommodate its vertical movement for breech access.

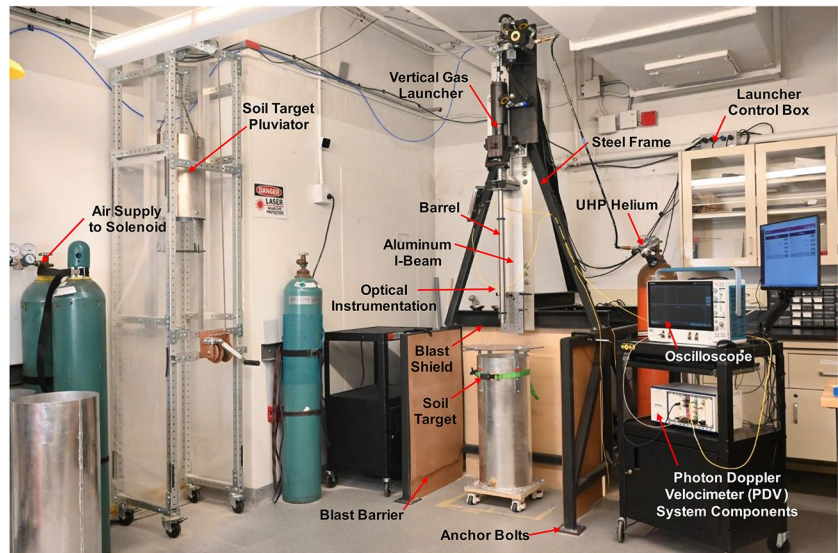
A rigid, passively isolated frame was designed in-house for vertical mounting of the launcher. The frame was designed to support the launcher mass as well as the anticipated recoil and resulting vibrations caused by gas release from operating the launcher. The frame was fabricated primarily from steel. A 2.2 m long aluminum I-beam supported the launcher and provided adequate space and mounting options for optical and magnetic instrumentation. The launcher was bolted onto an aluminum plate, which was in turn mounted onto the I-beam. The overall launcher length was 3.0 m, with a base footprint of 1.5 m × 1.0 m. The structural components of the frame were 50.8 mm square steel section with a thickness of 1.29 mm, welded to form the frame shown in Fig. 5. Erection of the rigid frame from the welded assemblies was completed through the advantageous use of bolted connections for ease

of transportation and constructability. The frame was anchor-bolted into the floor slab to ensure sufficient rigidity during ballistic experiments. The frame was painted matte black to limit the reflection of laser light during experiments. Plywood and cardboard sheets were clamped to the rigid frame to contain the sand ejecta, which, if not contained, could lead to time-intensive cleanup, as well as damage to the velocity measurement instrumentation. Preliminary tests revealed that the muzzle blast affected the soil surface and the ballistic response of the projectile. These adverse effects were empirically mitigated by loosely fitting the target chamber with a polycarbonate blast shield. The shield was placed at approximately 10 cm from the target chamber rim to accommodate unrestricted cavity expansion. The main components of the vertical frame design are depicted in Fig. 5.

Soil Targets

A challenging aspect of ballistic tests in soils is the preparation of well characterized and reproducible targets [18]. In this study, uniform silica sand targets were prepared by pluviating dry 50–80 Ottawa sand into a cylindrical barrel. The sand was a poorly-graded fine material, passing the #50 sieve and retaining on the #80 sieve. The target containers were fabricated from aluminum and were fitted with casters for movement. Each container was 0.76 m tall with a diameter of 0.31 m. The pluviator was constructed by suspending a hopper on a pulley system connected to a rigid aluminum frame. Shutters and wire screen diffusers were mounted inside of the hopper depending

Fig. 5 Components of the experimental setup



on desired soil target density. Dry sand was pluviated into the soil target drum from a predetermined height.

The factors that affect the density of a sample are the falling height of the sand, porosity of the shutters, and presence of wire screen diffusers [19]. Two sample densities were obtained for both loose and dense conditions. Dense samples were prepared by permitting sand to fall at an empirically-determined slow rate, allowing particles to reach terminal velocity before depositing into the target chamber. This was accomplished using a shutter porosity, *i.e.* the ratio of the opening area to the total area of the hopper base, of approximately 1%. The shutters were supplemented with two wire screen diffusers offset by 45°. The hopper was raised to its maximum height of approximately 1.8 m. Loose samples were prepared by raining sand at a higher rate, using an empirically-determined shutter porosity of 28%. To prepare loose samples, the hopper height was maintained at a constant minimum height of approximately 75 cm, being raised using a winch after each layer was pluviated. No wire screen diffusers were used in preparing loose samples in conjunction with shutters designed with a high porosity to facilitate the large quantity of sand raining. Further details of the pluviator design and sample preparation can be found in Giacomo et al. [20] and Kenneally et al. [21].

Launcher Performance and Ballistic Experiments

Muzzle Velocity Measurements

The gas launcher efficiency and pressure–velocity response were determined in initial trial shots by varying the launcher reservoir pressure and measuring the resulting

muzzle velocity. The dimensions and mass of the projectiles were selected as scaled versions of typical unexploded ordnance encountered in Formerly Used Defense Sites (FUDS). Blunt and conical nose cylinders were machined from aluminum projectiles (6061T6 aluminum alloy) to a mass of 34.5 g and length-to-diameter ratio of 5.33, which corresponds to a scaled mass of the M107 155-mm howitzer high explosive artillery. Additional cylindrical rod projectiles were also machined from aluminum and stainless steel to a mass of 16.4 g and 96.5 g, respectively, in order to investigate the mass-dependence of the launcher performance. The blunt nose aluminum projectile having a mass of 34.5 g was used for comparison of nose shape effects. The conical projectiles had an apex angle of 60°, a diameter of 14.30 mm, and a length-to-diameter ratio of 5.33.

Muzzle velocity is an important measurement made in ballistic experiments, which can be controlled by adjusting the chamber reservoir pressure. Measurements can be made using several instrumentation methods. The muzzle velocity and the soil target impact velocity were approximately the same, as confirmed by high-speed camera and PDV records. Further details are provided in the next sections.

High-Speed Camera A high-speed camera was utilized to acquire images of the projectiles in-flight once it exited the muzzle. The projectiles used to measure the muzzle velocity were 85 mm long conical projectiles having a diameter of 14.30 mm, machined from both stainless steel and aluminum. The stainless steel and aluminum projectiles had a mass of 96.5 g and 34.5 g, respectively. The high-speed camera was a NAC Memrecam HX5 equipped with a Nikon Nikkor 50 mm f/1.2 fast prime lens, used at maximum aperture. A close-up filter (Hoya 82 mm HMC) was added to the

lens to improve the image coordinate to physical coordinate conversion. A frame rate of 40 kHz and shutter speed of 5 μ s were used. The experimental setup used with the high-speed camera is shown in Fig. 6. Two 500 W tungsten light sources were used to front-illuminate the setup, and a white diffuse sheet was placed behind the field of view of the camera to provide better contrast during projectile flight.

Sample images captured of an aluminum cone-cylinder projectile are displayed in Fig. 7. Images from the high-speed camera were analyzed using the open-source software ImageJ to compute the distance between frames over a known time interval. A fiducial image was captured prior to each experiment in order to calculate the conversion factor from image coordinates to physical coordinates. The highspeed camera captured a field-of-view equivalent to approximately 50 mm of projectile flight upon exiting the muzzle. For each experiment with highspeed footage, the moving average velocity was calculated by using three successive frames. The mean moving average velocities and corresponding standard deviations were calculated in Table 1 for six launcher pressures. The muzzle velocity resolution using highspeed footage was calculated as 2.5 m/s.

Magnetic Sensors Muzzle velocity of steel projectiles was independently measured using magnetic proximity sensors. Two passive variable reluctance speed (VRS) magnetic speed sensors (Honeywell 3050A13) were mounted in series adjacent to the projectile trajectory near the muzzle (Fig. 8a). VRS magnetic sensors operate by measuring changes in the magnetic field in the vicinity of the sensor as a ferrous metal moves past it. A magnet in the sensor generates a fixed magnetic field. Two sensors were placed at a distance of 25.4 mm from each other, as shown in Fig. 8,

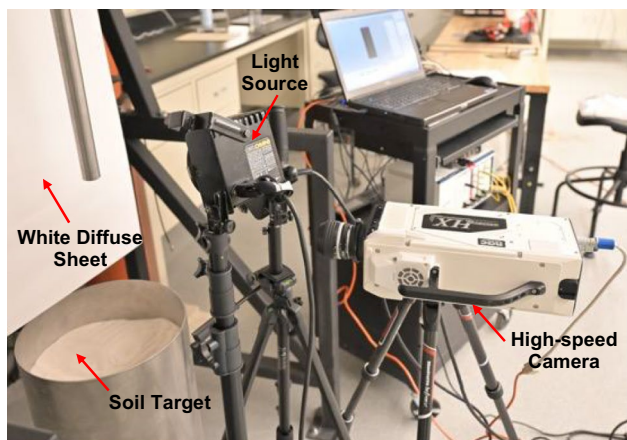


Fig. 6 High-speed camera experimental setup to measure muzzle velocity

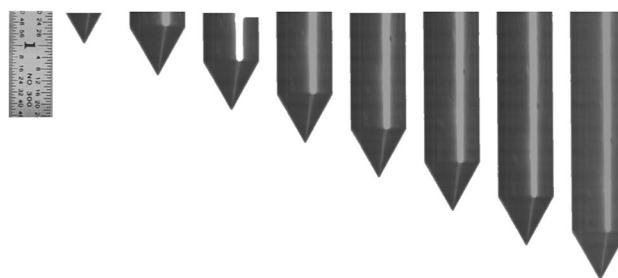


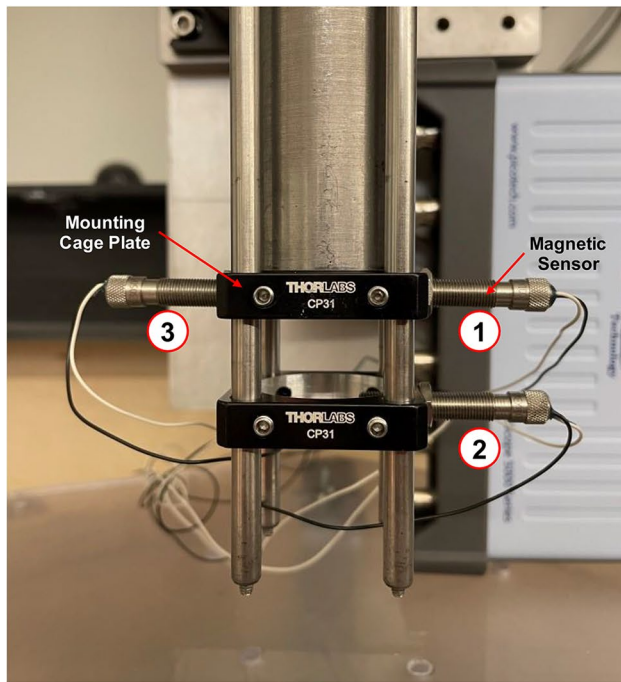
Fig. 7 Sequence of images captured from high-speed camera to measure muzzle velocity μ . The interframe time in the experiment was 25 μ s

each of which was used to record an independent measurement of velocity. The sensors were mounted to cage plates (Thorlabs CP31) on the outside of the launcher barrel. A third sensor was placed on the opposite side of one of the cage plates and was used to trigger an oscilloscope. Sensors were placed in cage plates, which were in turn mounted on precision-machined guide rods. All three sensors were positioned along the path of the projectile, such that the sensing area at the tip of the sensors was at a distance of approximately 2 mm from the side of the projectile. As the projectile passed by each sensor, the flux of the magnetic field increased sharply. This change in magnetic field strength induced a current into a coil winding which was attached to the output terminals of the magnetic sensors. The current was amplified using a dedicated data acquisition system (Picoscope 5444D).

A time plot of waveforms resulting from the three magnetic sensors in an experiment is shown in Fig. 8b. As the projectile approached each magnetic sensor, the change in magnetic flux generated an electric signal. Subsequent passage of the projectile nose and shank continued to generate a signal with alternating positive and negative amplitudes. Once the projectile back end passed the sensor, a final positive or negative signal was generated. The time delay between the signal peaks recorded in the two sensors was

Table 1 Measured muzzle velocity for a projectile having mass of 34.5g using highspeed video footage

Chamber Pressure (bar)	Mean Moving Average Velocity (m/s)	Standard Deviation (m/s)
40	158	2.68
50	177	2.09
70	202	2.83
100	221	2.19
130	249	1.58
150	262	3.62



(a)



(b)

Fig. 8 (a) Magnetic sensors mounted at the muzzle to measure projectile velocity; (b) Typical signals obtained from the three magnetic sensors

used to compute the muzzle velocity, given the distance between the magnetic sensors. A data acquisition system was used to record the signals at a sampling rate of 5 MS/s. The magnetic sensors were mounted to the barrel using cage plates with a custom-drilled 6.35 mm diameter hole. A signal was first recorded as the projectile nose aligned with a given magnetic sensor. It can be seen that sensors one and three (labeled in Fig. 8a), which were positioned at the same elevation, recorded a signal rise at identical times, while

sensor two began recording a signal with a delay of approximately 0.234 ms. Given the vertical distance of 25.4 mm between signals one and two, the time delay of 0.234 ms corresponds to a calculated projectile velocity of 109 m/s. Each of the three sensors continued to record a current from changes in their magnetic field while the projectile shank traveled past the sensor. Therefore, an independent calculation of projectile velocity could be made by dividing the projectile length of 76.2 mm by the time duration of the recorded signal. The projectile velocity computed from the three sensors following the latter approach was 108 m/s, 111 m/s, and 108 m/s, respectively. The mean velocity from the four measurements was 109 m/s, with a standard deviation of 1.73 m/s. This velocity is commensurate with calibrated velocity measurements of 110 m/s for a steel rod projectile at the experimental chamber pressure of 50 bar, as further discussed in the next sections.

Photogate Sensor A separate custom-made (Aeolus Devices) speed meter was designed and mounted on the muzzle of the barrel, as shown in Fig. 9. The sensor comprised three equidistant photogates placed along the projectile axis. The photogates consisted of an infrared emitter and a phototransistor receiver. Uninterrupted light from the emitter to the receiver resulted in a strong signal. When the projectile passed through each of the photogates, the light signal was disrupted. The three photogates were equidistantly spaced at 50 mm. The projectile muzzle velocity was determined from the known distance between photogates and the time delay between signal interruptions. Further details on photogate speedmeters can be found in Cave et al. [16].

Photon Doppler Velocimetry (PDV) Muzzle velocity and penetration velocity measurements were also made using a single channel PDV. This measurement technique is based on the Doppler effect, and uses frequency variations in laser light source reflected from the moving projectile to resolve its velocity [22–24]. PDV resolves the difference between the frequencies of Doppler shifted and source light, known as the beat frequency. The beat frequency, f_b , is a function of the velocity of the projectile and the wavelength of the light source. To resolve the velocity–time history, the beat frequency is calculated as [25]:

$$f_b(t) = 2 \times \left[\frac{v(t)}{c} \right] \times f_0 = 2 \times \left[\frac{v(t)}{\lambda_0} \right] \quad (1)$$

where c is the speed of light, λ_0 is the wavelength of the source light, and v is the speed of the reflector. The optical beat signal collected from the PDV instrumentation was converted to an electric signal, and was analyzed using a fast oscilloscope (Tektronix MSO64 6-Series). The intensity spectrum of the signal was computed using a short-time

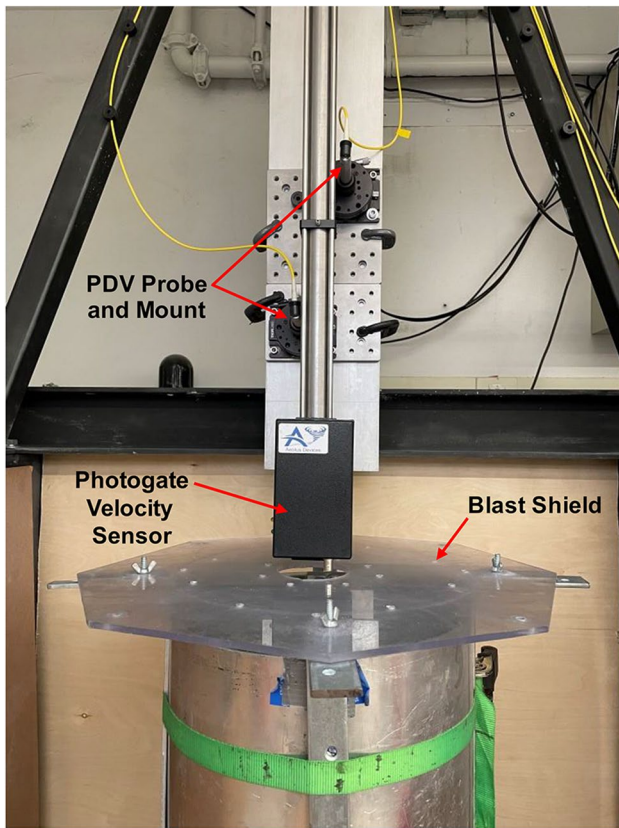


Fig. 9 Speed meter used for velocity measurements

Fourier transform. The analysis was conducted in the MATLAB toolbox SIRHEN, which used a discrete Fourier transform along with a window function to extract frequency components from a finite number of beat signal data points. The peak of the intensity spectrum for a time interval was taken as the beat frequency [26]. The beat frequency from this signal is proportional to the velocity of the object through the following relationship:

$$v(t) = \frac{1}{2} \times \lambda_0 \times f_b(t) \quad (2)$$

A collimator probe served as both the source light and collection point of Doppler shifted light. The probe was mounted to an optical breadboard secured to the aluminum I-beam. Fiber optic cables connected the probe to the PDV instrumentation. A coherent laser light source with a wavelength of 1550 nm was used to reflect light from the projectile at the muzzle and during flight. Retroreflective tape was mounted to the back of each projectile to reflect Doppler-shifted light in the same direction as its incident wave for data collection. A range of retroreflective tapes were tested for their signal return strength [22, 27]. A *Telemecanique XUZB11* retroreflective tape was used in all of the experiments reported herein.

The muzzle velocity calibration methods previously described were utilized to both independently measure muzzle velocity and confirm measurements from PDV. It is noteworthy that the PDV, unlike other muzzle velocity measurement methods, provided continuous velocity measurements even after projectile impact and penetration into the soil target. An example of a PDV signal during projectile flight and subsequent impact and penetration into the soil target is shown in Fig. 10. The data was collected from an aluminum projectile with a muzzle velocity of 150 m/s launched into dense dry sand.

The PDV probe line of sight was aligned to reliably detect the projectile prior to impact. There was no need to correct for the negligible deceleration between muzzle exit and impact. Single integration of the velocity–time history captured from PDV revealed the distance travelled by the projectile. For the test reported in Fig. 11, it was determined that the projectile travelled approximately 70 mm from first detection of PDV signal to the point of impact. The average velocity of the projectile during free-flight was calculated to describe the difference between muzzle and impact velocities. It can be seen that the muzzle and impact velocities are within the standard deviation of this measurement region. In-flight velocities from the experiment in Fig. 11 were also within the muzzle velocity error measured in Table 1. This confirmed the negligible differences between muzzle and impact velocities, as well as the feasibility of using the previously described instrumentation methods to verify velocity measurements from PDV.

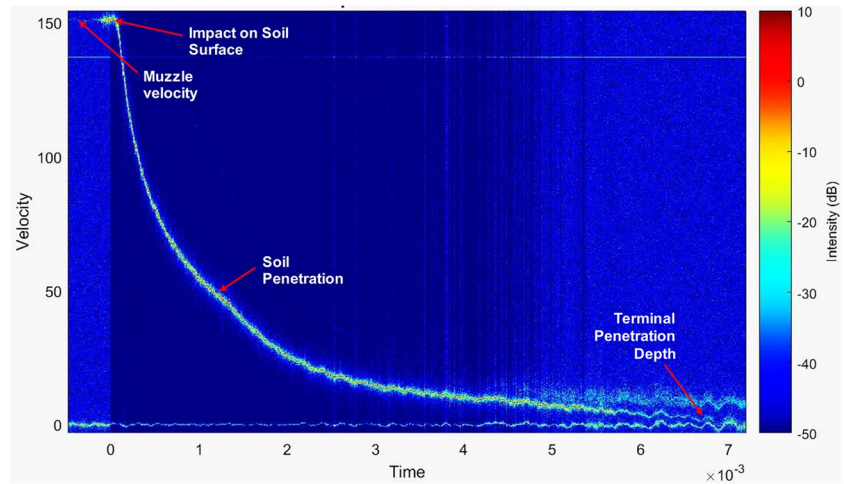
Theoretical Muzzle Velocity and Launcher Efficiency

The muzzle velocity of the launcher was predicted using the theoretical relationship for isentropic ideal gas expansion. Comparison of theoretical and measured muzzle velocities can be used to define the launcher efficiency. The equation of conservation of energy was used in conjunction with the governing equation for isentropic expansion of helium gas in the launcher barrel. The projectile potential energy and the energy required for the expansion of gas behind the projectile in the barrel was assumed to be equal to the projectile kinetic energy. The energy equilibrium for isentropic expansion of gas in the barrel could therefore be described as follows:

$$\frac{mv^2}{2} = W_{gas} + mgl_b \quad (3)$$

where m is the mass of the projectile, g is the acceleration due to gravity, and l_b is the length of the barrel. W_{gas} is the work performed by expansion of a gas as a function of its pressure and volume at any point during expansion, and can

Fig. 10 Velocity–time history obtained from PDV. Muzzle velocity was measured as 150m/s



be written as, $W_{gas} = \int p dV$, where p is the instantaneous pressure and dV is the instantaneous volume. According to Boyle's law for isentropic conditions, the term pV^γ is a constant, where V is the volume of the compressed gas and γ is the specific heat ratio, which is 1.66 for helium. The work performed by the gas, W_{gas} , can therefore be written as:

$$W_{gas} = \frac{P_0 V_0}{\gamma - 1} \left[1 - \left(\frac{V_0}{V_0 + A l_b} \right)^{\gamma - 1} \right] \quad (4)$$

where P_0 and V_0 are the supplied pressure and volume of the pressure chamber prior to projectile launch. Substituting Eq. (4) in Eq. (3) and rearranging the resulting equation yields the muzzle velocity, v . An efficiency factor, η , is introduced to correct for losses, resulting in,

$$v = \eta \sqrt{\frac{2 P_0 V_0}{m \gamma - 1} \left[1 - \left(\frac{V_0}{V_0 + A l_b} \right)^{\gamma - 1} \right] + 2 g l_b} \quad (5)$$

A finite difference form of Eq. (5) was implemented, with l_b taken as the independent variable representing the distance traveled by the projectile in each increment as it traveled the length of the barrel. The maximum value of l_b was set to the barrel length, that is, 1.2 m. Figure 12a illustrates the predicted theoretical velocity of a 34.5 g projectile through the barrel with varying chamber pressure. Figure 12b demonstrates the predicted theoretical velocity of projectiles fired at 70 bar having masses of 96.5 g, 34.5 g, and 16.4 g. The finite difference incremental implementation of Eq. (5) reveals that the projectile velocity gain decreases as it travels through the barrel, and approaches a plateau near the muzzle of the 1.2 m smooth-bore barrel used in this study. This plateau is more noticeable as launcher pressure and projectile mass decrease. While increasing the barrel length can further increase the muzzle velocity, the available laboratory headroom limited the barrel length of the vertical range to approximately 1.2 m.

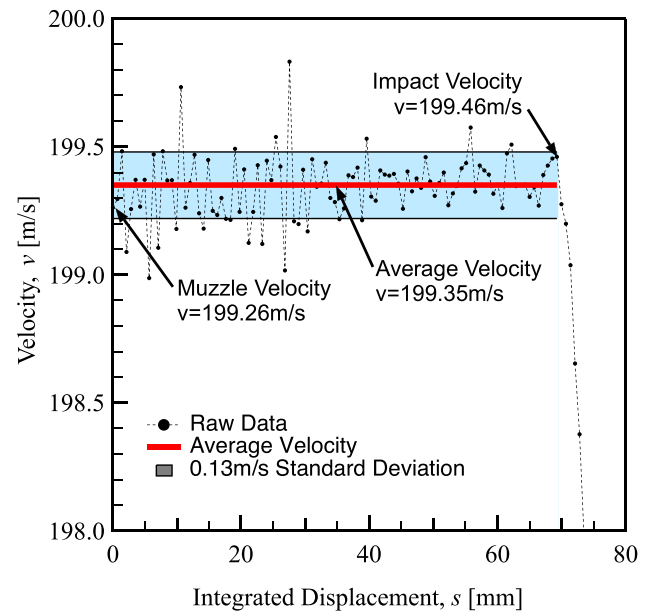


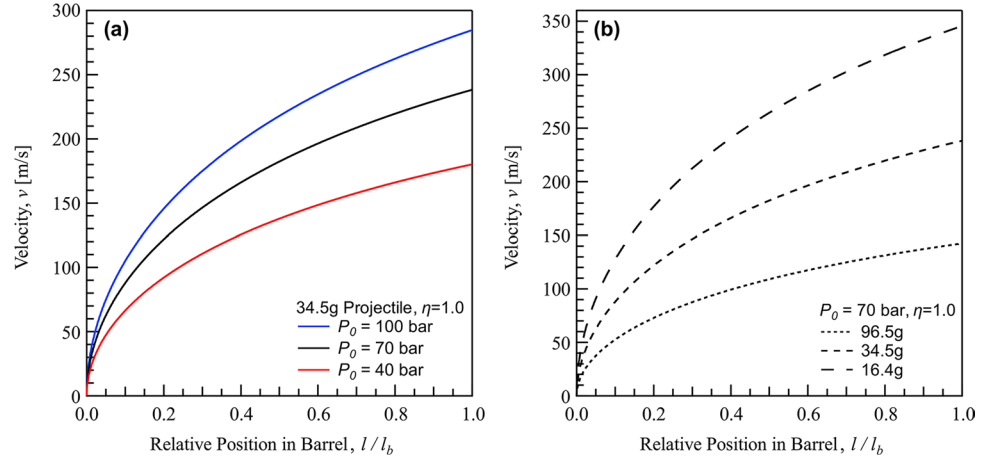
Fig. 11 PDV measurements demonstrating continuity between muzzle and impact velocities

Launcher Efficiency According to Eq. (5), there is a square root relationship between the efficiency and the pressure-mass ratio. A square root best-fit of experimental data can be represented as follows:

$$\eta = 100 - \mu \sqrt{\frac{P_0}{m}} \quad (6)$$

where μ is a constant determined from best-fit analysis. Equation (6) calculates launcher efficiency, η as a percent for a given pressure-mass ratio, P_0/m , where P_0 is the reservoir pressure and m is the projectile mass. It can similarly be shown that the velocity-efficiency ratio, v/η , scales linearly

Fig. 12 Projectile velocity gain within barrel shown for (a) 34.5g projectile, (b) 70bar chamber pressure, assuming no efficiency reduction factor



with the square root of P_0/m , and the data for the three projectiles can be described as follows:

$$\frac{v}{\eta} = \psi \sqrt{\frac{P_0}{m}} \quad (7)$$

where ψ is a best-fit constant. Substituting Eq. (6) into Eq. (7) and rearranging the terms to solve for v yields the calibrated velocity curve for a gas launcher, which may be written as

$$v = 100\psi \sqrt{\frac{P_0}{m}} - \mu\psi \frac{P_0}{m} \quad (8)$$

Equation (8) uses launcher-unique calibrated values of μ and ψ to calculate the velocity of the gas launcher in this study as a function of projectile mass and reservoir pressure. The reservoir pressure and projectile mass calibration limits of the launcher can be defined by the boundary conditions of Eq. (8). The trivial condition is when P_0 is equal to zero; this indicates that the system is not pressurized, and the projectile will remain at rest. The second boundary condition is the base pressure of 25 bar; the minimum pressure required to properly operate the shuttle valve. Equation (8) is capable of predicting muzzle velocities lower than 25 bar, however, the launcher is physically unable to operate as predicted below this chamber pressure. The upper calibration limit can be determined by evaluating the first derivative of Eq. (8) at a value of zero. The first derivative of Eq. (8) is as follows:

$$\frac{dv}{d\left(\frac{P_0}{m}\right)} = \frac{50\psi}{\sqrt{\frac{P_0}{m}}} - \mu\psi \quad (9)$$

Theoretical muzzle velocities predicted using Eq. (5) were compared to experimentally measured velocities to quantify the launcher efficiency, η , defined as the ratio of measured velocity to theoretical velocity. The results are shown in Fig. 13 for the three projectiles tested. Launcher efficiency was highest

at the lowest tested pressures, and it decreased as the reservoir pressure increased. The highest efficiency was computed for the 96.5 g projectile at the lowest pressure, at 92%. The decrease in efficiency at higher pressures can be attributed to helium gas leakage through the shuttle valve design used. The efficiency dropped by an average of approximately 12% as reservoir pressure increased from 40 to 150 bar. The launcher was more efficient for the heaviest projectile (96.5 g), with an average efficiency of 87% over the pressures tested. The lightest projectile tested (16.4 g) was the least efficient, with an average efficiency of approximately 74%.

The nonlinear relationship between reservoir pressure and muzzle velocity for all projectiles tested was fitted with a second order polynomial fit with reasonable accuracy, as shown in Fig. 13d. These second order polynomial fits were extrapolated to a base pressure of 25 bar; the minimum pressure required to properly operate the shuttle valve.

Muzzle Velocity Calibration and Repeatability

The calibration curves along with the experimental data reported in previous sections were used to calibrate the launcher pressure required, given muzzle velocity and projectile mass. Results of the pressure–velocity calibration experiments are shown in Fig. 14. While the calibration is only valid for the launcher parameters tested, the approach described above can be used for calibration of similar launchers having different barrel length, diameter, and pressurized gas used.

The experimental launcher efficiency, η , expressed as a percent, was determined from the ratio of experimental muzzle velocity reported in Fig. 13 to theoretical muzzle velocities calculated from Eq. (5). Likewise, the pressure-mass ratio, P_0/m , was calculated for each ballistic experiment. Experimental efficiency measurements were plotted against the pressure-mass ratio for each experiment as shown

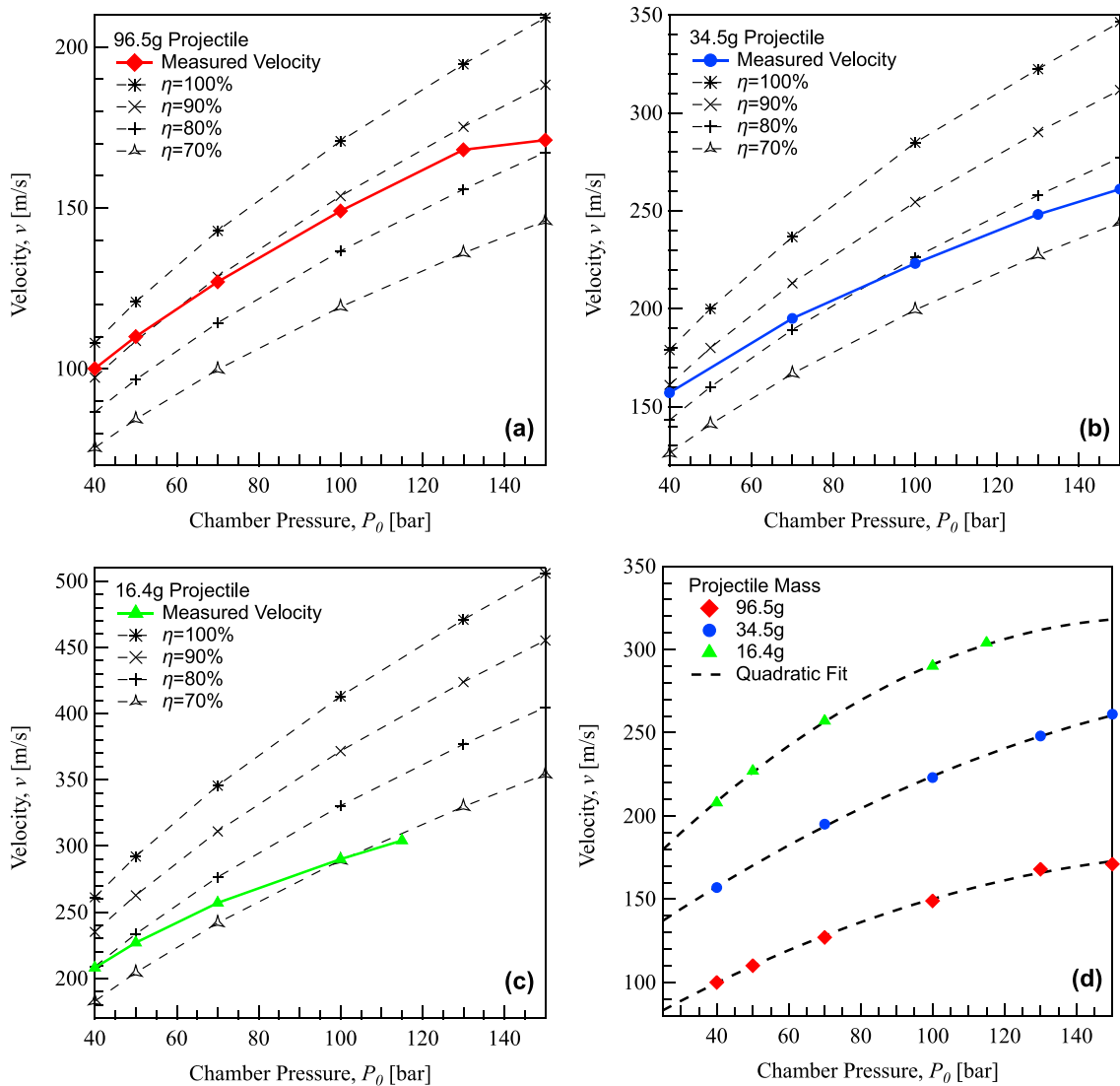


Fig. 13 Theoretical versus experimental pressure versus velocity for the (a) 96.5g projectile, (b) 34.5g projectile, (c) 16.4g projectile, and (d) quadratic fits of curves for projectiles having masses of 96.5g, 34.5g, and 16.4g

in Fig. 14a. The experimental data using the three projectile masses of 16.4 g, 34.5 g, and 96.5 g tested exhibit a quadratic relationship between efficiency and P_0/m , as predicted by Eq. (5). The efficiency of the launcher was therefore found from Eq. (6) with a μ constant of 12. A best-fit value of 1.67 was found for ψ using the projectiles tested.

The resulting fit using Eq. (8) and values for μ and ψ reported above is shown in Fig. 14c. It can be seen that Eq. (8) accurately captures the velocity–pressure relationship of the launcher with a relative standard deviation of less than 1.2%. Setting Eq. (9) equal to zero reveals a maximum calibrated P_0/m of 17.36 bar/g. The parameters of μ and ψ calibrated the launcher in this study to an extrapolated maximum velocity of 348 m/s and corresponding efficiency of 50%. Since μ and ψ will be unique to each launcher,

maximum calibrated pressure–mass ratios between launchers will vary. It is evident that efficiency decreases significantly at higher P_0/m ratios. Nevertheless, Eq. (8) can be used to predict the required reservoir pressure for a given projectile mass and a target muzzle velocity.

Muzzle Velocity Repeatability The launcher calibration experiments described in previous sections were used to specify chamber pressures needed to launch scaled versions of projectiles commensurate with typical warfare ordnance. Projectile impact velocities in the range of 150–200 m/s are typically of interest in UxO applications. Over the course of experimental campaigns, enough data was obtained to quantitatively evaluate the variance in gun performance. The results of the velocity repeatability measurements are

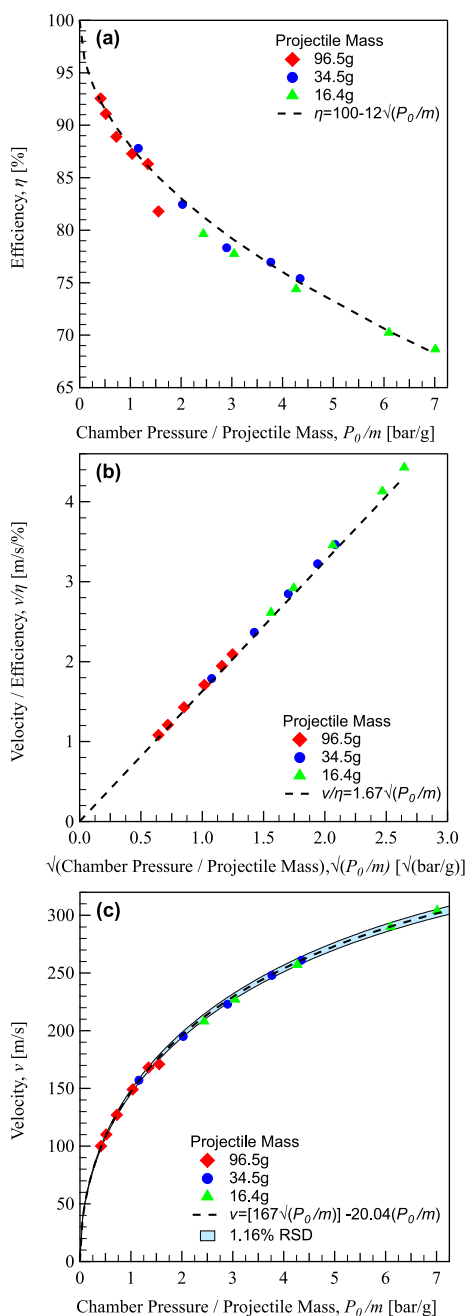


Fig. 14 Calibrated launcher curves as functions of (a) efficiency with pressure-mass ratio, (b) velocity-efficiency ratio with pressure-mass ratio, (c) velocity with pressure-mass ratio

displayed in Table 2. The standard deviation of the muzzle velocity was on average 1.93 m/s with a relative standard deviation of 1.16% for projectiles travelling at 150–200 m/s, confirming the high repeatability of the setup and data acquisition method. The slight variations in impact velocity were primarily attributed to the use of a manual pressure gauge and systematic uncertainty within the data acquisition system.

Projectile Diameter Tolerance Effects

The role of projectile diameter tolerance, that is, the clearance between the projectile and the inner bore of the launcher barrel, on muzzle velocity was investigated. Projectiles having mass of 34.5 g were precision machined to several diameters of 14.25 mm, 14.30 mm, 14.35 mm, and 14.40 mm. The four projectiles were launched at pressures of 40 bar, 70 bar, and 100 bar.

Results are shown in Fig. 15, superimposed with the relative standard deviation of the launcher and the experimental curve determined in Fig. 13a. Results of the launcher efficiency versus diameter tolerance are summarized in Table 3.

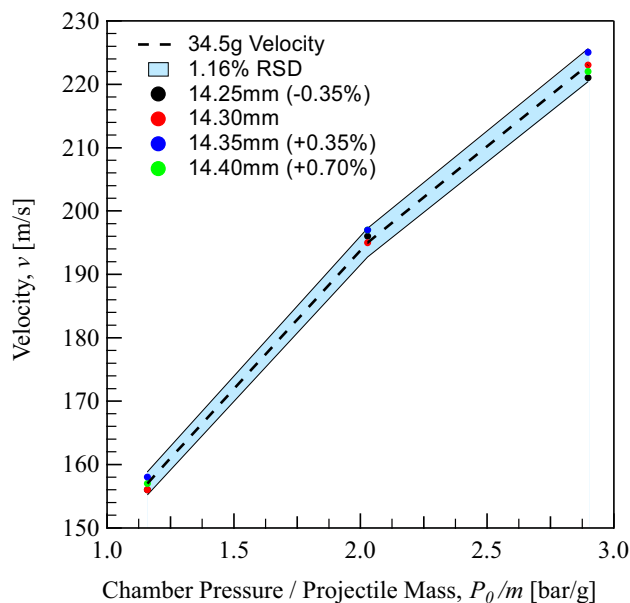


Fig. 15 Launcher pressure versus velocity for the 34.5g projectile launched with varying diameter tolerance

Table 2 Quantified velocity error for launcher experiments at selected velocities

Projectile Mass (g)	Chamber Pressure (bar)	Average Velocity (m/s)	Standard Deviation (m/s)	Relative Standard Deviation (RSD)
34.5	36	150.85	1.72	1.14%
34.5	72	200.23	2.24	1.12%
96.5	100	150.00	1.83	1.22%
Average			1.93	1.16%

Table 3 Quantified efficiency variation for launcher experiments with varying diameter tolerance

34.5 g Projectile Diameter (mm)	Diameter Tolerance	Launcher Efficiency		
		40 bar	70 bar	100 bar
14.25	-0.35%	86.3%	82.3%	77.5%
14.30	N/A	86.5%	81.9%	78.3%
14.35	+0.35%	87.4%	82.9%	79.1%
14.40	+0.70%	87.4%	82.8%	78.0%
Efficiency Range		1.1%	1.0%	1.7%
Relative Standard Deviation (RSD) of Efficiency		0.67%	0.58%	0.89%

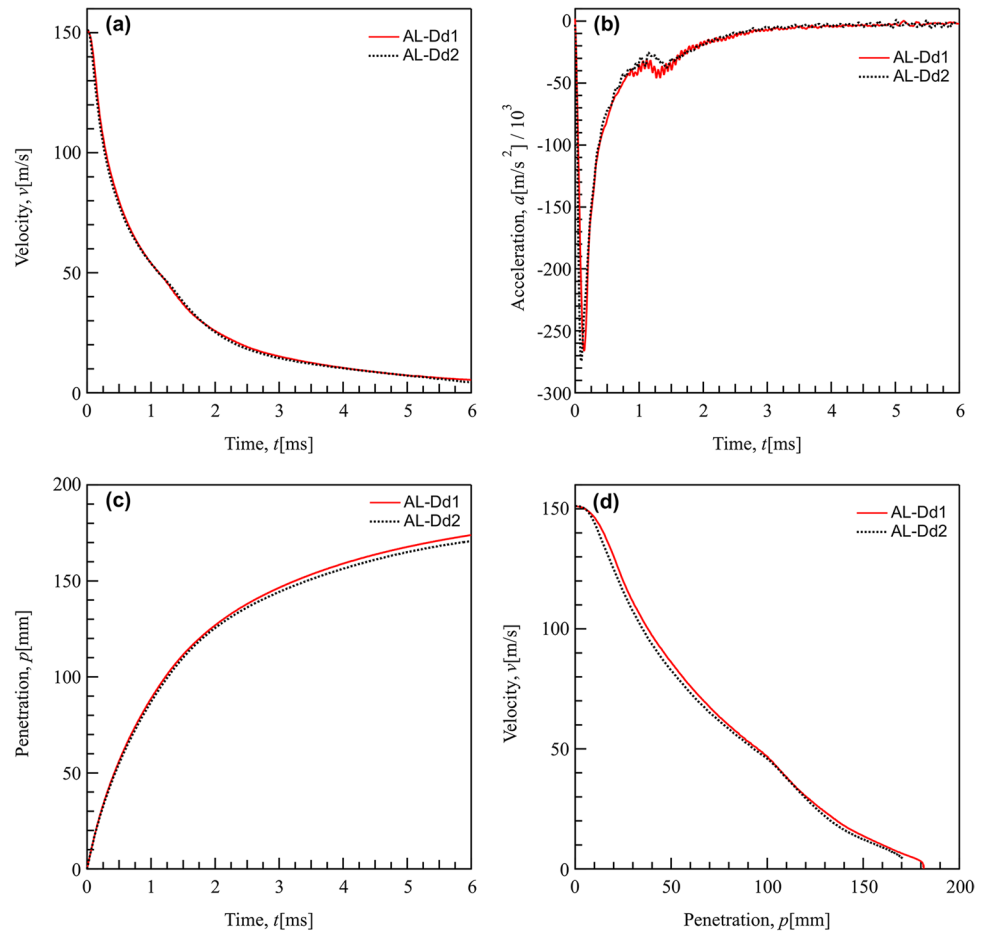
It was determined that both the muzzle velocities and launcher efficiencies measured for the four varying diameter tolerances were within the relative standard deviation of the launcher, indicating that muzzle velocity was insensitive to projectile diameter tolerance, within the investigated range.

Ballistic Experiments in Sand

The operation of the launcher and associated apparatus is illustrated with ballistic experiments conducted with 60-degree conical tip projectiles penetrating into dense dry sand targets at an impact velocity of 150 m/s. The projectiles were fabricated from 6061-T6 aluminum and had a mass

of 34.5 g. The soil target had a bulk density of 1.76 g/cm^3 . The PDV setup described in previous sections was used to collect velocity data from the projectile in the soil target. The launcher was operated at a pressure of 36 bar (Table 2). The time history of the beat signal from the PDV instrumentation was used to compute the instantaneous velocity of the projectile. This resulting velocity–time history was differentiated to produce the acceleration data of the projectile. Similarly, integration of the velocity–time history yields the penetration data of the projectile. The acceleration data was noisy across all experiments. Data smoothing was required to expose intrinsic properties of the signal without diminishing the value of peak deceleration, as described in

Fig. 16 Repeatability of reported experiments, shown for penetration of 34.5g conical nose projectiles in dense dry sand. (a) velocity–time; (b) penetration–time; (c) acceleration–time; (d) velocity–penetration



Omidvar et al. [22, 28]. The velocity–time, acceleration–time, penetration–time, and velocity–penetration histories are shown in Fig. 16. It can be seen that the PDV signal was able to follow the back of the projectile from in-flight to the depth of burial in the soil target, demonstrating the efficacy of PDV for such applications. This also suggests that the projectile had little to no angle of attack upon impact and subsequent penetration, or that any minor angle of attack was corrected for during penetration. Otherwise, line-of-sight access would have been compromised. Furthermore, it can be seen that the experiments were highly repeatable in all stages of penetration.

Concluding Remarks

Design and performance of a laboratory apparatus based on a gas gun capable of launching projectiles into soil targets was successfully demonstrated in this study. Details of the launcher configuration optimized for the vertical launch of projectiles into soil targets were presented. Scaled versions of large artillery were launched at velocities representative of unexploded ordnance of practical concern.

The launcher featured a free-floating shuttle valve to rapidly release UHP helium from the reservoir, along with a fast-acting solenoid valve. The launcher was calibrated for use with ultra-high-purity helium (UHP) as a propellant. The results of the study underscored the reliability of multiple velocity measurement techniques and the remarkable consistency of muzzle velocity data across a range of projectile masses and tolerances. Furthermore, the study quantified the launcher's efficiency by comparing the measured muzzle velocities with theoretical values predicted through equations governing the isentropic expansion of helium gas. These findings established the launcher efficiency within a range of 70–90% for the projectiles tested.

Critical data was gathered using a laser photon Doppler velocimeter (PDV) mounted adjacent to the launcher barrel, enabling the tracking of projectile velocity both before impact and during penetration into the soil target. Various additional techniques were presented to confirm impact velocities and calibrate the pressure–velocity curve for the vertical launcher. A pluviator was employed to prepare soil targets having precise and highly repeatable bulk densities. This apparatus facilitated the measurement of gravity-aligned penetration velocity into the soil targets. Consequently, the experimental results not only serve as a basis for determining the depth of burial of projectiles in soil targets, but also can provide valuable insights for the development and calibration of penetration models rooted in soil resistance dynamics.

Acknowledgements The authors gratefully acknowledge the support of the Strategic Environmental Research and Development Program (SERDP) of the United States of America, Grant No: MR19-1277. Technical support from Sydor Technologies is gratefully acknowledged.

Data Availability All data, models, and code generated or used during the study appear in the submitted article.

References

1. Iskander M, Bless S, Omidvar M (2015) *Rapid Penetration in Granular Media*. Elsevier
2. Omidvar M, Iskander M, Bless S (2014) Response of Granular Media to Rapid Penetration. *Int J Impact Eng* 66:60–82. <https://doi.org/10.1016/j.ijimpeng.2012.03.004>
3. Ruiz Suarez JC (2013) Penetration of Projectiles into Granular Targets. *Rep Prog Phys* 76(2013):066601
4. Rogers JA, Bass N, Mead PT, Mote A, Lukasik GD et al (2022) The Texas A&M University Hypervelocity Impact Laboratory: A Modern Aeroballistic Range Facility. *Rev Sci Instruments* 93:085106. <https://doi.org/10.1063/5.0088994>
5. Allen WA, Mayfield EB, Morrison HL (1957) Dynamics of a Projectile Penetrating Sand. *J Appl Phys* 28(3):370–376. <https://doi.org/10.1063/1.1722750>
6. Bless SJ, Berry DT, Pedersen B, Lawhorn W (2009) Sand Penetration by High-Speed Projectiles. *AIP Conf Proc* 1195(1):1361–1364. <https://doi.org/10.1063/1.3295061>
7. Borg JP, Morrissey M, Perich C, Vogler T, Chhabildas L (2013) In Situ Velocity and Stress Characterization of a Projectile Penetrating a Sand Target: Experimental Measurements and Continuum Simulations. *Int J Impact Eng* 51:23–35
8. Glößner C, Moser S, Külls R, Heß S, Nau S, Salk M, Penumadu D, Petrinic N (2017) Instrumented Projectile Penetration Testing of Granular Materials. *Exp Mech* 57(2):261–272. <https://doi.org/10.1007/s11340-016-0228-0>
9. Karcz JS, Bowling D, Cornelison C, Parrish A, Perez A, Raiche G et al (2016) The Ames Vertical Gun Range. In: 47th Lunar and Planetary Science Conference. Houston, TX, USA; 2016. abstract 2599
10. See TH, Cardenas F, Montes R (2012) The Johnson Space Center Experimental Impact Lab: Contributions Toward Understanding the Evolution of the Solar System. 43rd Lunar and Planetary Science Conference. Houston, TX, USA; 2012. Abstract #2488
11. Kawai N, Zama S, Takemoto W, Moriguchi K, Arai K, Hasegawa S, Sato E (2015) Stress Wave and Damage Propagation in Transparent Materials Subjected to Hypervelocity Impact. *Procedia Engineering* 2015(103):287–293
12. Price MC, Cole MJ, Harriss KH, Alesbrook LS, Burchell MJ et al (2024) A New Compact, Self-Compressing, Vertical One and Two-Stage Gas Gun at the University of Kent. *Int J Impact Eng* 184:104828
13. Zhong T, Liu X, Zhang YY, Chen S, Zhang BB, Tao Y et al (2021) Penetration Dynamics of a Carbonate Sand: A synchrotron Phase Contrast Imaging Study. *Int J Impact Eng* 152:103839
14. USACE (2021) Formerly Used Defense Sites (FUDs). Los Angeles District, U.S. Army Corps of Engineers, <https://www.spl.usace.army.mil/Missions/Formerly-Used-Defense-Sites/>. Accessed 29 June 2024
15. Department of Defense Office of the Under Secretary of Defense for Acquisition and Sustainment (2020) *Defense Environmental Programs Annual Report to Congress*. 22p

16. Cave A, Roslyakov S, Iskander M, Bless S (2014) Design and Performance of a Laboratory Pneumatic Gun for Soil Ballistic Applications. *Exp Tech* 40:541–553
17. Grace D, Mercurio S, Omidvar M, Bless S, Iskander M (2022) A Vertical Ballistics Range with Photon Doppler Velocimeter Instrumentation for Projectile Penetration Testing in Soils. Conference Proceedings of the Society for Experimental Mechanics Series, 93–100
18. Kenneally B (2021) Analytical Modeling of High Velocity Penetration in Sand. *Thesis*. Manhattan College, Riverdale, New York
19. Rad N, Tumay M (1987) Factors Affecting Sand Preparation by Raining. *Geotechnical Testing J* 10(1):31–37 (ASTM)
20. Giacomo L, Dinotte J, Omidvar M (2023) Resistance of dry and partially saturated sand to rapid Ordnance penetration using photon doppler velocimetry. *Geo-Congress 2023*:293–302. <https://doi.org/10.1061/9780784484708.027>
21. Kenneally B, Omidvar M, Bless S, Iskander M (2021) Observations of Velocity-Dependent Drag and Bearing Stress in Sand Penetration. In: *Dynamic Behavior of Materials, Volume 1: Proceedings of the 2020 Annual Conference on Experimental and Applied Mechanics*. Pp. 29–35
22. Omidvar M, Dinotte J, Giacomo L, Bless S, Iskander M (2024) Photon Doppler Velocimetry for Resolving Vertical Penetration into Sand Targets. *Int J Impact Eng* 185:104827
23. Peden R, Omidvar M, Bless S, Iskander M (2014) Photonic Doppler Velocimetry for Study of Rapid Penetration into Sand. *Geotechnical Testing J* 37(1). <https://doi.org/10.1520/GTJ20130037>
24. Mercurio S, Grace D, Bless S, Iskander M, and Omidvar M (2024) Frequency-Shifted Photonic Doppler Velocimetry (PDV) for Measuring Deceleration of Projectiles in Soils. Springer Nature, *Acta Geotechnica*. <https://doi.org/10.1007/s11440-024-02252-9>
25. Dolan DH (2020) Extreme Measurements with Photonic Doppler Velocimetry (PDV). *Rev Sci Instrum* 91(5):051501
26. Ao T, Dolan DH (2010) SIRHEN: A Data Reduction Program for Photonic Doppler Velocimetry Measurements. Sandia National Laboratories. Report No. SAND2010–3628
27. Lagoski JT (2009) Retroreflector for Photon Doppler Velocimetry. MS Thesis. Air Force Institute of Technology, Wright-Patterson Air Force Base, Ohio.
28. Omidvar M, Dinotte J, Giacomo L et al (2024) Dynamics of sand response to rapid penetration by rigid projectiles. *Granular Matter* 26:73. <https://doi.org/10.1007/s10035-024-01440-4>

Publisher's Note Springer Nature remains neutral with regard to jurisdictional claims in published maps and institutional affiliations.

Springer Nature or its licensor (e.g. a society or other partner) holds exclusive rights to this article under a publishing agreement with the author(s) or other rightsholder(s); author self-archiving of the accepted manuscript version of this article is solely governed by the terms of such publishing agreement and applicable law.